Boundary-Layer Meteorol (2009) 132:261–277
DOI 10.1007/s10546-009-9395-1

ARTICLE

Analysis of Model Results for the Turning of the Wind and Related Momentum Fluxes in the Stable Boundary Layer

Gunilla Svensson · Albert A. M. Holtslag

Received: 21 September 2008 / Accepted: 14 May 2009 / Published online: 5 June 2009

Abstract The turning of wind with height and the related cross-isobaric (ageostrophic) flow in the thermally stable stratified boundary layer is analysed from a variety of model results acquired in the first Global Energy and Water Cycle Experiment (GEWEX) Atmospheric Boundary Layer Study (GABLS1). From the governing equations in this particular simple case it becomes clear that the cross-isobaric flow is solely determined by the surface turbulent stress in the direction of the geostrophic wind for the quasi-steady state conditions under consideration. Most models indeed seem to approach this relationship but for very different absolute values. Because turbulence closures used in operational models typically tend to give too deep a boundary layer, the integrated total cross-isobaric mass flux is up to three times that given by research numerical models and large-eddy simulation. In addition, the angle between the surface and the geostrophic wind is typically too low, which has important implications for the representation of the larger-scale flow. It appears that some models provide inconsistent results for the surface angle and the momentum flux profile, and when the results from these models are removed from the analysis, the remaining ten models do show a unique relationship between the boundary-layer depth and the surface angle, consistent with the theory given. The present results also imply that it is beneficial to locate the first model level rather close to the surface for a proper representation of the turning of wind with height in the stable boundary layer.

Keywords Ageostrophic flow · Cross-isobaric flow · Ekman equations · GABLS · Inertial oscillation · Momentum fluxes · Stable boundary layer · Wind direction

G. Svensson (✉)
Department of Meteorology, Stockholm University,
106 91, Stockholm, Sweden
e-mail: gunilla@misu.su.se

A. A. M. Holtslag
Meteorology and Air Quality Section, Wageningen University,
Wageningen, The Netherlands

1 Introduction

In operational weather forecast and climate models, the turning of the wind in the stably stratified boundary layer is often much smaller than in reality. This is, for instance, found for the ECMWF (European Centre for Medium-Range Weather Forecasts) model in comparison with tower observations at Cabauw and Lindenberg (e.g. Bosveld and Beyrich 2004). Such results have important implications for dispersion calculations in the stably stratified boundary layer (Angevine et al. 2006). The directional shear in the lowest layers of the atmosphere is often also underestimated in models, which is important for plume spread (e.g. Walcek 2002). In addition, the decay of synoptic-scale cyclones is largely determined by the frictional inflow in the boundary layer in combination with the secondary spin-down effect (Holton 2004; Beare 2007). Thus, it is important to obtain the correct magnitude of the cross-isobaric (ageostrophic) flow in combination with the depth of the turbulent layer.

The overall goal of GABLS (Global Energy and Water Cycle Experiment (GEWEX) Atmospheric Boundary Layer Study) is to improve the understanding of the atmospheric boundary layer and its representation in regional and large-scale climate models (Holtslag 2003, 2006). The first study, GABLS1, concerned a simple shear-driven stable boundary layer case with a cooling surface and a moderately strong background wind. A detailed discussion of the large-eddy simulation (LES) intercomparison can be found in Beare et al. (2006) and the mean single-column model results are discussed in Cuxart et al. (2006, hereafter CUX06).

The aims of our study are to further analyse the results of a variety of single column models that were used in GABLS1, and also to explore aspects of the turbulence closure schemes that determine the turning of the wind within the stable boundary layer. It appears that in the various model results from GABLS1, large differences occurred for the calculated angle between the surface and geostrophic winds. In our analysis, we also use results from the LES for GABLS1 (Beare et al. 2006).

The set-up of GABLS1 intercomparison case is based on LES simulations presented by Kosovic and Curry (2000), which in turn were loosely based on observations taken in October in the Arctic region. Thus, as in CUX06, we here use the LES results as a reference. The main conclusion from the LES intercomparison (Beare et al. 2006) was that the 11 participating LES codes were all able to simulate the case with reliable statistics. Convergence in the statistics was reached for a grid resolution of 3.125 m and finer, while the solutions of the calculations using 6.25 m were within $\pm 20\%$ of the higher resolution results. Sensitivity to the different subgrid models used was also found but the overall averaged momentum and buoyancy profiles resembled the well-known profiles presented in Nieuwstadt (1984, 1985). Therefore, in CUX06 and in the present study, we use the averaged results from the eight LES codes that were run at the 3.125-m resolution for comparison.

The GABLS1 single-column models include first-order and higher-order closures (prognostic turbulent kinetic energy), in both operational and research models. In CUX06, the evolution of the boundary layer was studied in detail and the main conclusion was that the operational models have a much higher mixing efficiency than the research models, resulting in a deeper boundary layer. In fact, many of the research models simulated too much mixing, at least when compared to the LES results. The sensitivity of the schemes to the closure parameters was partly explored in CUX06.

In this paper, we analyse the model results in more detail with a focus on the turning of the wind at the surface and the height-integrated cross-isobaric mass flux. The system of equations used can be simplified to the well-known set of Ekman equations (Ekman 1905) that are solved numerically on a one-dimensional vertical grid for a quasi-steady state. As such we are able to construct a number of theoretical constraints in this particular case that

the models should fulfil (Sect. 2). The differences obtained for the various models are therefore solely a result of the differences in turbulence closure and/or numerical representations. Note that such a study is not that simple when using field data because of the varying atmospheric and surface conditions and the difficulty of estimating the geostrophic forcing. The set-up of the model intercomparison and basic results are given in Sect. 3; Sect. 4 provides a further analysis of the results and discusses modelling implications, while Sect. 5 provides conclusions.

2 Background

The basic boundary-layer equations are derived from the Navier–Stokes equations after introducing a separation between the mean and turbulent flow, and by further neglecting horizontal turbulent flux divergence and molecular viscosity. Using the definition of the geostrophic wind, we have the following set of equations describing the flow (e.g. Stull 1988; Holton 2004):

$$\frac{d\overline{u}}{dt} = f(\overline{v} - v_g) - \frac{\partial \overline{u'w'}}{\partial z}, \tag{1}$$

$$\frac{d\overline{v}}{dt} = -f(\overline{u} - u_g) - \frac{\partial \overline{v'w'}}{\partial z}, \tag{2}$$

where $\overline{u}$ and $\overline{v}$ are the mean horizontal wind components, f is the Coriolis parameter, $\overline{u_g}$, $\overline{v_g}$ are the components of the geostrophic wind and $\overline{u'w'}$, $\overline{v'w'}$ are the components of the turbulent stress aligned with $\overline{u}$ and $\overline{v}$, respectively.

Around sunset when turbulence in the unstable boundary layer reduces rapidly, horizontal pressure gradients tend to accelerate winds towards the geostrophic value. Due to the Coriolis force, however, an inertial oscillation is introduced within (damped) and above (undamped, or nearly so) the stable boundary layer (SBL) (e.g., Blackadar 1957; Stull 1988). As such, super-geostrophic values near the top of the SBL are typically formed later at night, as is evident in the formation of the low-level jet. The inertial oscillation that is present above the SBL, and can be seen in single-column model studies (as we will see later in this paper), may be difficult to observe due to large-scale influences and other damping mechanisms (e.g., Lundquist 2003).

For the stable boundary layer, the above equation system can be solved analytically in the stationary and horizontal homogeneous case and by using simple expressions for the turbulent stresses. Assuming a constant eddy coefficient, K_m, the solution is easily obtained (Ekman 1905; Stull 1988). However, this solution is unphysical both at the surface and at the interface with the free tropospheric flow, and several alternative analytical solutions with more realistic functions for the eddy coefficient can be found in the literature (e.g. Nieuwstadt 1985; Grisogono and Oerlemans 2001; Tan 2001; Parmhed et al. 2005).

By orienting the coordinate system so that the geostrophic wind is along the x-axis, we obtain in the stationary and horizontal homogeneous case an equation for the cross-isobaric flow, $\overline{v}$:

$$f\overline{v} = \frac{\partial \overline{u'w'}}{\partial z}. \tag{3}$$

Thus, given the above assumptions, cross-isobaric (ageostrophic) flow only exists if a turbulent stress divergence is present, i.e. in the boundary layer. It is interesting to note that a

linear decrease of the momentum flux (in the direction of the geostrophic wind) with height implies a constant $\overline{v}$ according to Eq. 3. Integrating vertically over the atmosphere gives:

$$f \int_0^\infty \overline{v} dz = -\overline{u'w'}_0, \tag{4}$$

so that the vertically integrated cross-isobaric flow (or the cross-isobaric mass flux when Eq. 4 is multiplied by density) depends only on the turbulent surface stress along the x-axis, $\overline{u'w'}_0$, i.e. the surface stress in the direction of the free tropospheric wind.

Since Eq. 3 implies that the v component is zero unless there is turbulent stress divergence, it is helpful to divide the integral of Eq. 4 into two parts:

$$f \int_0^h \overline{v} dz + f \int_h^\infty \overline{v} dz = -\overline{u'w'}_0, \tag{5}$$

where h is the turbulent boundary-layer height, and above this height the turbulent momentum flux should vanish or be very small. Consequently, the second integral on the left-hand side of Eq. 5 equals zero (or is at least small).

Note that the right-hand side of (5) can also be written as $-\overline{u'w'}_0 = u_*^2 \cos\alpha$ where α is the surface angle, e.g. the angle between the surface stress (or the wind near the surface) and the geostrophic wind. Furthermore, u_* is the surface friction velocity (defined formally by $u_*^4 = (-\overline{u'w'}_0)^2 + (-\overline{vw'}_0)^2$), so (5) can also be written as:

$$f\, h\, \langle \overline{v} \rangle \;=\; u_*^2 \cos\alpha, \tag{6}$$

where $\langle \overline{v} \rangle$ is the averaged cross-wind component in the turbulent boundary layer. Thus Eq. 6 indicates that the averaged cross-wind component in the boundary layer is directly related to the angle between the surface stress and the geostrophic wind for given values of boundary-layer depth and surface stress.

3 Basic Results

3.1 GABLS1

Model results as presented in CUX06 are further analysed herein, together with the averaged LES results for 3.125-m resolution (Beare et al. 2006). The models were run for 9 h in both studies, assuming that this was sufficient time to reach steady state. The stably stratified condition was reached by initializing with a 100-m deep near-surface neutral layer and a potential temperature increase of 0.01 K m^{-1} above, and then applying a surface-cooling rate of 0.25 K h^{-1}. The geostrophic wind was held constant at 8 m s^{-1}, the latitude specified as 73°N ($f = 1.39 \times 10^{-4}\ s^{-1}$), and the surface roughness was set to 0.1 m and radiation schemes were turned off. This set-up resulted in a quasi-steady state with a surface Obukhov length, L, of 149 m for the averaged LES, and a boundary-layer height, h, of approximately 180 m. Thus $h/L = 1.2$ for the boundary layer is achieved, which is a moderately stable case (e.g. Nieuwstadt 1984; Holtslag and Nieuwstadt 1986).

Nineteen models participated in the single-column intercomparison study, ranging from operational models with first-order closure and a vertical resolution having six grid points within the first 400 m (minimum vertical grid), to higher-order closure models with the

same resolution as the main LES experiment (6.25 m, the suggested resolution for the single-column models). For a description of the individual models and the mean results from the study, we refer to CUX06. Note that in the set of single-column models, h is defined for each model as the level at which the total momentum flux is 5% of the surface value, divided by 0.95 (as in CUX06).

In this study, we focus on the overall difference between the participating operational models and research models. As such, we do not identify each individual model but display them in the figures as four groups, notably: operational models with first-order closure (five models), operational models with higher-order closure (prognostic turbulent kinetic energy, two models), research models with first-order closure (two models), and research models with higher-order closure (nine models). One model (referred to as SandiaLabs in CUX06) was excluded in the study because it is completely different in its design, is never used in a meteorological full-scale model and lacks many of the results needed for the analysis. In combination with the single-column model results, we use the averaged LES results (3.125-m resolution).

The reason why the various models use different methods for their turbulence parameterisation is not easy to unravel, and is most likely partly due to historical reasons and to various tuning exercises, and partly to the extent that models have been critically evaluated with observations in the past, as well as decisions made on the complexity that atmospheric turbulence and the boundary layer should be represented. In fact, with the GABLS model inter-comparison studies, the aim is to understand the basis for the various parameterisations and to make a critical evaluation of the various schemes.

Figure 1 reproduces the mean LES results (after Beare et al. 2006), as well as the results for the individual column models (after Cuxart et al. 2006), for the mean potential temperature and the total wind speed. The total turbulent fluxes of momentum (denoted by τ, as defined by $\tau^2 = (-\overline{u'w'})^2 + (-\overline{vw'})^2$) and sensible heat (denoted by $\overline{\theta' w'}$) are also shown. It is clear that the depth of the turbulent layer varies quite significantly between the different model solutions, with the operational models giving the deepest layers. For temperature, all models agree at the surface, since the surface temperature was prescribed, but large differences are seen in the inversion region (Fig. 1a).

The magnitudes of the surface heat flux vary quite substantially (Fig. 1b), but the profiles show approximately a linear decrease of flux with height. The heights to the maximum in the modelled total wind speed (the low-level jet, Fig. 1c) also show a large variation consistent with the variations in boundary-layer depth. The magnitudes of the jet are 1–2 m s^{-1} greater than the background geostrophic wind (8 m s^{-1}), and the total momentum flux also shows large differences in magnitude for the different deep layers (Fig. 1d). In summary, all model results show approximately the same type of structure of the boundary layer but with very different boundary-layer depths. For further discussion and details regarding these GABLS results we refer to Beare et al. (2006) and Cuxart et al. (2006).

3.2 The Ekman Spiral and Cross-Isobaric Flow

All models that participated in GABLS1 produce the Ekman spiral, as can be seen in Fig. 2. The model results line up with the operational models having the least turning of the wind in the boundary layer, followed by the LES placed in the middle of the research model results. The lowest 10%, or the surface-layer, part of the solution is shown in Fig. 2 with dotted lines. It is clear that this layer is resolved with a variable number of grid levels (dots in the figure), from zero in the surface layer to six points. Note also that some turning with the wind occurs

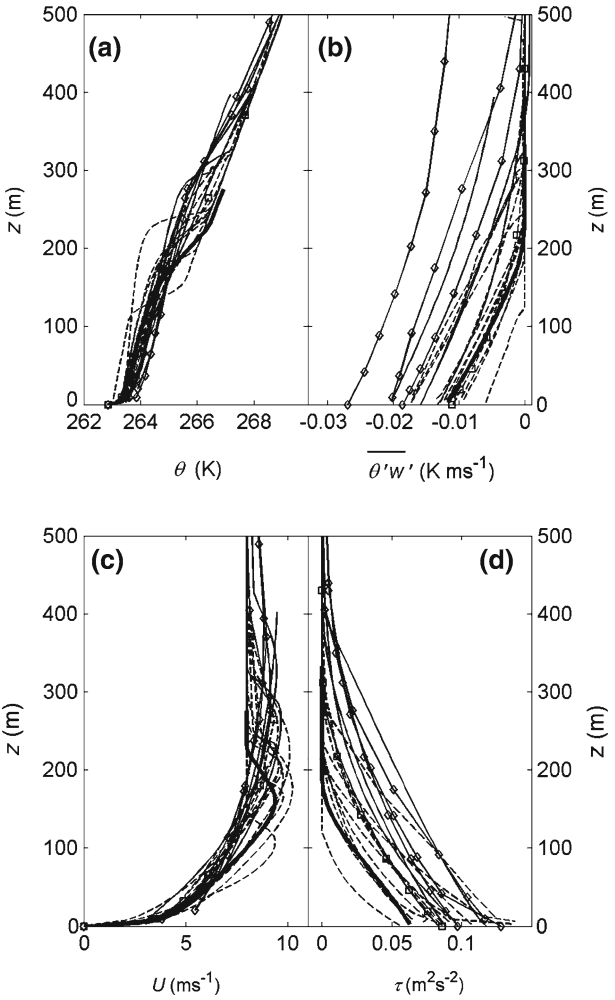

Fig. 1 Model results for **a** potential temperature, **b** turbulent heat flux, **c** total horizontal wind speed and **d** turbulent momentum flux for operational models (*solid lines*), research models (*dashed lines*) and averaged results for LES (*thick solid line*). Model results are adapted from Beare et al. (2006) and Cuxart et al. (2006)

within the surface layer in most models. The shape of the spirals in Fig. 1 depends on how the turbulent stress is parameterised, which varies significantly among the participating models (CUX06).

All models produce a super-geostrophic wind close to the boundary-layer top, consistent with the analytical solution and the discussion in Sect. 2, though some models do not return to the geostroptic wind above 400 m (Fig. 1c). An obvious reason for this is a constant angular momentum oscillation (Holton 2004) in the free troposphere that is caused by e.g. the initialization procedure. A disturbance in the free troposphere will continue to exist as an oscillation in the free troposphere if there are no damping processes. As can be seen in Fig. 3, this is indeed the case for (at least) one of the participating models (Andrén 1990; model

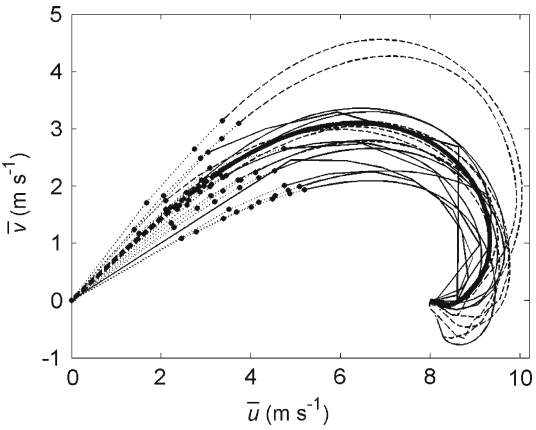

Fig. 2 Hodographs for the operational models (*solid lines*), research models (*dashed lines*) and averaged results for LES (*thick solid line*). The surface-layer part (lowest 10%) of the boundary layer is shown as dotted lines and here the larger black dots indicate the various model levels

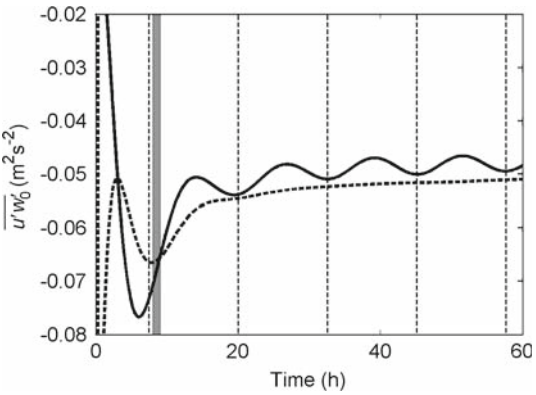

Fig. 3 Results from one single-column model for the terms of Eq. 4: The surface stress component in the direction of the geostrophic wind (*dashed line*) and the integrated cross-isobaric wind component times the Coriolis factor (*solid line*). The *vertical dashed lines* illustrate the inertial period and the shaded region indicates the time interval applied in the intercomparison study (Cuxart et al. 2006)

acronym Stock 1 in CUX06). Here, we have run the model for 60 h and evaluated the two terms in Eq. 4.

During the initialization, the height of the boundary layer is estimated as a first guess as $h = 0.2u_* f^{-1}$, in this case about 400 m, and the wind is assumed to vary log-linearly in this layer. The disturbance above the steady-state boundary layer then continues to oscillate around the geostrophic value; this is seen in the integrated cross-isobaric wind (solid line, Fig. 3). Fortunately, the period of the oscillation is such that the two terms in Eq. 4 are approximately equal during hour 9, which is the period evaluated in this study.

To examine if the actual cross-isobaric mass flow relates to the surface value of the momentum flux in the direction of the geostrophic wind, we have evaluated the integral in Eq. 4 for all models (Fig. 4). The integral is first performed over the entire reported model domain, since any deviations from the background geostrophic wind must originate from the boundary layer (or possibly from the initialization procedure, see above). However, the difference compared with evaluating the integral over only the boundary-layer depth is, for most models, very small with one exception (see below). The v component is thus indeed only non-zero within the boundary layer (as defined using the momentum flux). For each model, the integral value is plotted against both the surface value and the lowest model layer since some models have large discrepancies between these values (see above). If the models agree the theory, the results lie on the 1:1 line. Reasons for deviations from the line include uncertainty in

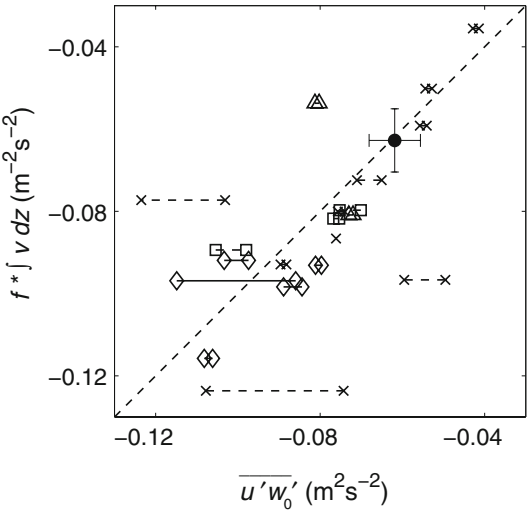

Fig. 4 The integrated cross-isobaric wind component plotted against the turbulent stress (at the two lowest model layers connected with a line) in the direction of the geostrophic wind for all participating models in GABLS1 (see Eqs. 4 and 5). Operational models with first-order closure (*diamonds*), operational models with higher-order closure (*triangles*), research models with first-order closure (*squares*), higher-order research models (*crosses*), and averaged LES result with standard deviations (*filled circle with error bars*)

the integration (vertical discretization), and influences by an inertial oscillation in the wind above the boundary layer (as in Fig. 3). However, since the database only contains results from hours 8 and 9, it is not possible to evaluate the latter part for all the individual models. Most model results are rather close to the 1:1 line but there are also large deviations in both directions. This issue is further explored and discussed below in Sect. 4.

Figure 5a shows the variation of the cross-isobaric wind component within the boundary layer, with the maximum cross-isobaric wind varying between 2 and 4.5 m s^{-1}, while the LES gives a maximum of 3.1 m s^{-1}. Not only variations in the maximum are seen, but also the profile shapes are different. The scatter is not reduced if the profiles are scaled with their maximum value and the turbulent boundary-layer height (not shown). The height of the maximum varies between 20% and 80% of the boundary-layer height for the various models with the operational models peaking at lower scaled heights. The average LES profile has a maximum slightly below the middle of the turbulent layer.

3.3 The Surface Angle and the Momentum Flux

As can be seen in Fig. 2, the magnitude of the surface angle (the angle between the near-surface and geostrophic winds) varies substantially among the models (see also Table IV, CUX06). The averaged LES result has a surface angle of 36° while the operational models vary between 23 and 36°. The surface angle averaged over all research models is 36°, which agrees well with the averaged LES result but the variation is substantial (27°–46°). It is interesting to note that van Ulden and Holtslag (1985) found, by analysing the Cabauw data, an average turning angle of about 35° across the moderately stable boundary layer, which is consistent with the current LES (and averaged research) model results.

It turns out that the surface angle is directly related to the depth of the turbulent boundary layer h, and in Fig. 6 the calculated boundary-layer height for each model is plotted as a function of the corresponding surface angle. It is seen that deeper (shallower) boundary layers have smaller (larger) surface angles, as is also implied by Eq. 6 for a given surface stress and for a given cross-wind averaged over the boundary layer, $\langle \overline{v} \rangle$. However, there is

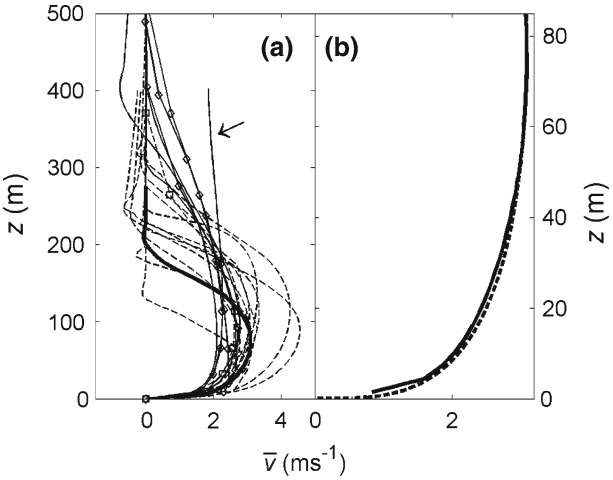

Fig. 5 Cross-isobaric wind component (ms^{-1}) as a function of height (m) for **a** the models in the intercomparison study, operational models (*thin solid lines*), research models (*dashed lines*) and, averaged LES results (*thick solid line*); **b** Profiles of averaged LES results (*thick solid line*) and by expression (8) (*dashed line*) for the lower part of the SBL. Most models are run with a grid resolution of 6.25 m but a few used their operational grid (grid levels shown with symbols for these models). One of the model results discussed in the text is indicated with an *arrow*

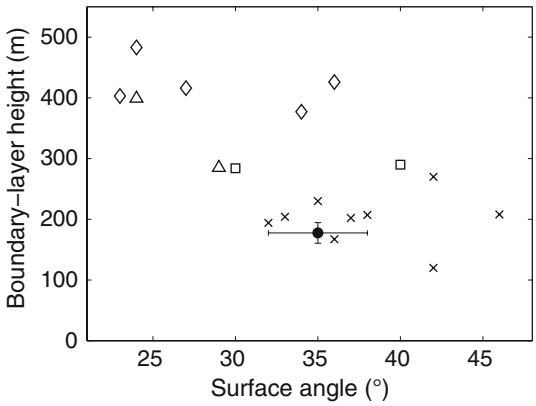

Fig. 6 The angle between the surface wind and the geostrophic wind plotted against the boundary-layer height (m, for definition see the text). Symbols as in Fig. 4

considerable scatter in Fig. 6, which seems to be related to the variation of $\langle\overline{v}\rangle$ (see Fig. 5a) and the surface stress (see Fig. 1d) among the various models.

Let us examine this further. As concluded earlier, the momentum flux component in the direction of the geostrophic wind should not decrease linearly with height, since this implies a constant $\overline{v}$ component throughout the entire layer (see Eq. 3). However, one of the operational models does give that result as can be seen in Fig. 5a (line pointed out by an arrow). The corresponding $\overline{u'w'}$ profile can be seen in Fig. 7a (also line pointed out by an arrow), which indeed is very close to linear throughout the layer except close to the surface.

In any case it is clear from Fig. 7a that most models provide a $\overline{u'w'}$ profile that is quite linear through the bulk of the boundary layer, and with convex curvature close to the ground. In all cases the $\overline{u'w'}$ profiles approach zero asymptotically towards the top of their respective boundary layers. For the same background conditions the various parameterisation schemes

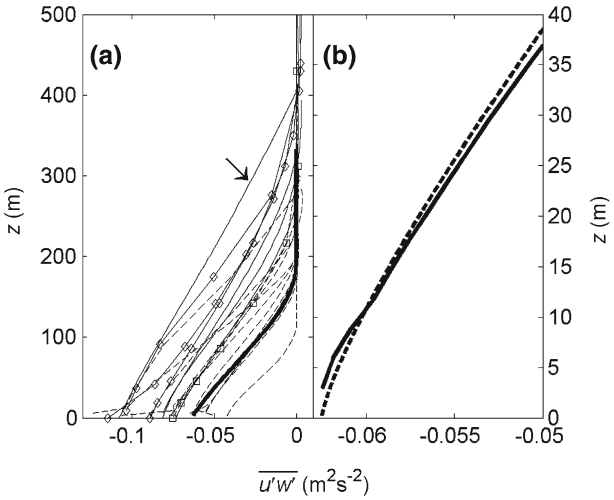

Fig. 7 Turbulent stress in the direction of the geostrophic wind ($m^2 s^{-2}$) with height (m) for the individual models in the intercomparison study, **a** operational models (*thin solid line*), research models (*dashed line*) and, averaged LES results (*thick solid line*); **b** averaged LES results (*thick solid line*) and curve given by Eq. 9 for the lower part of the boundary layer. Most models are run with a grid resolution of 6.25 m and a few with operational grid (grid levels shown with symbols for these models). One of the model results discussed in the text is indicated with an *arrow*

give values at the surface between 0.04 and 0.12 $m^2 s^{-2}$, which is a factor-of-three spread (Fig. 7a); the corresponding LES value is 0.0625 $m^2 s^{-2}$. The operational models tend to be in the upper region of values due to the enhanced mixing (CUX06). Note that several models have a positive $\overline{u'w'}$ close to the top of the turbulent layer, consistent with a negative wind-speed gradient on the upper side of the jet.

Observations of the momentum flux and its variation with height for stably stratified conditions can be found in the literature (e.g. Caughey et al. 1979; Nieuwstadt 1984), and are often presented as a scaled total momentum flux. Thus, most model comparisons (e.g. Andrén 1990; Cuxart et al. 2006; Beare et al. 2006; Basu and Porté-Agel 2006) are also presented in terms of a scaled total momentum flux, often in combination with the well-known theoretical profile of Nieuwstadt (1984, 1985). For observations, the two stress components are normally not presented, at least not in a coordinate system defined by the geostrophic wind direction, as is necessary for the surface angle to be examined.

Note that in Nieuwstadt's theory the components of the momentum flux are not directly provided, but can be derived using the theoretical limit for the surface angle. However, the latter is predicted to become 60° (Nieuwstadt 1985) while the Ekman theory gives 45°. In fact neither of these values is consistent with observations of the wind turning with height in the stable boundary layer (van Ulden and Holtslag 1985; Bosveld and Beyrich 2004).

4 Further Analysis and Selection of Models

4.1 Momentum Fluxes

To further compare and understand the various model results, we have normalised the turbulent stress in the direction of the geostrophic wind with the surface value (or with the value

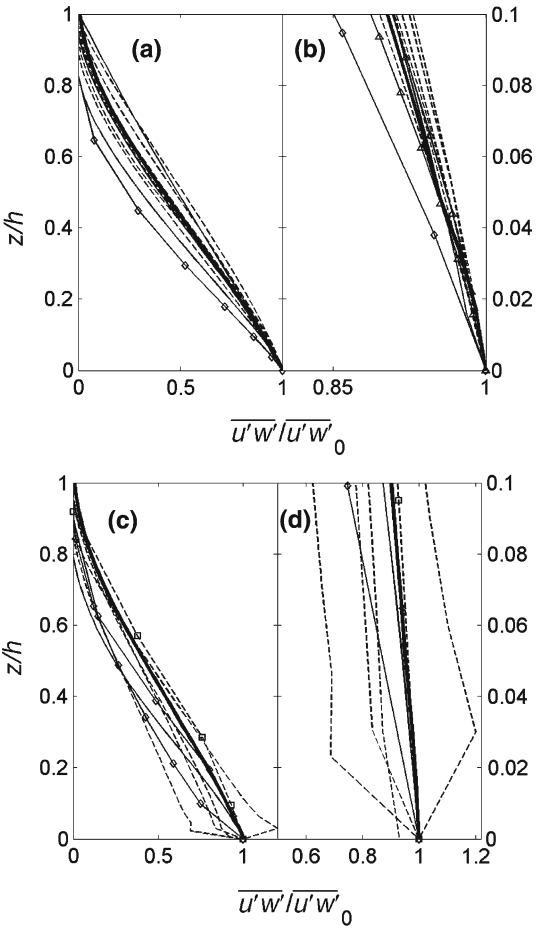

Fig. 8 Turbulent stress in the direction of the geostrophic wind normalised with its surface value versus relative height for the individual models in the intercomparison study. Model results are presented either in the upper or lower panels depending on the near-surface behaviour (see text for further explanation). Panels (**a** and **c**) for the entire boundary layer and panels (**b** and **d**) for the lower 10% of the boundary layer. Symbols as in Fig. 4

of the first model level available) and present it as a function of normalised boundary-layer height for each of the available single-column models. Results for the entire boundary layer are shown in Fig. 8a and c, and the results for the lowest 10% are given in Fig. 8b and d. By doing so we have identified two groups of models, namely those that show flux-profiles near the ground that clearly match with the boundary-layer profiles (Fig. 8a and b) and models that do not (Fig. 8c and d).

There may be several reasons for the unexpected behaviour in the lower panels of Fig. 8: first of all, errors may be present in the reported results and some of the model results may not yet be in equilibrium for the period analysed (see Fig. 3). Interestingly, with closer inspection, it turns out that for all of the models listed in the lower panels, the surface-flux formulation does not match the boundary-layer mixing approach. In such cases the surface friction does not match the momentum profile, and an anomalous shape of the near-surface part of the momentum profile is revealed (see Figs. 1d and 8c,d).

It is also important to realize that in the design of the model experiment the modellers were originally asked to use similarity theory with the *same* stability function for the surface layer (see CUX06). In retrospect this is somewhat unfortunate given the knowledge of current analysis. Thus, at least some of the inconsistency between the surface-flux formulation and

the boundary-layer mixing approach in some of the models has been artificially introduced. The use of the specified stability functions was not followed by six of the operational models (CUX06, Table IV) and these models do provide consistent results in the current analysis, stressing the importance of using surface-flux formulations that are consistent with the boundary-layer mixing scheme. Typically this is not too difficult for mixing schemes that are based on first-order flux-gradient relationships, but it may be troublesome for higher-order closure and TKE type schemes.

Note that some of the models in the lower panel have profiles very close to the mean LES profile, but they still have a mismatch with the surface value. This cannot be seen in the figure since only the surface friction is available, thus the surface value of $\overline{u'w'}$ cannot be included in the figure if the reported profiles did not include a surface value. For those models, the first level is translated to the surface in Fig. 8, even though it represents a certain height above the surface in the model.

Most simulations in Fig. 8 show a shape of the normalized momentum profile similar to the averaged LES results, some with more or less curvature. The same was already concluded for the total scaled momentum profiles in CUX06. Once again, it is clear from Fig. 8b that the operational models are to one side of the LES (c.f. Fig. 2). Note that one operational model has an almost linear profile throughout the boundary layer (Fig. 8a), and this is the model with the lowest surface angle (see Fig. 6).

4.2 Surface-Layer Behaviour

In all the models analysed, the turbulent momentum flux is parameterised (see CUX06 for exact expressions), using a turbulent eddy coefficient, K_m, and the wind gradient. In the equation of motion, Eq. 3, the cross-isobaric wind is given by the gradient of the turbulent momentum flux:

$$-f\overline{v} = \frac{\partial}{\partial z}\left(K_m \frac{\partial u}{\partial z}\right) = \frac{\partial K_m}{\partial z}\frac{\partial u}{\partial z} + K_m \frac{\partial^2 u}{\partial z^2}. \tag{7}$$

The cross-isobaric wind is thus dependent on the vertical gradient of the eddy coefficient and its actual value. (This can also be examined in Fig. 6a of CUX06.) Most of the model parameterisations use surface-layer theory for the turbulent eddy coefficient i.e. $K_m = ku_* z/\Phi_m$, and so the value of K_m should linearly decrease to zero when approaching the surface (certainly for the moderately stable conditions examined). This, however, appears not to be true for two of the research models of the turbulent kinetic energy (TKE) type, and we conclude that these models also have problems at the surface and these are therefore excluded in Fig. 8a and b.

By further analysing the model results, it appears that the cross-isobaric component at the surface is very sensitive to the vertical divergence of the momentum flux close to the surface. To illustrate this point it is convenient to revert to analytical formulations; as such we use the mean LES results of the v component up to its maximum value (at about 80 m) as our reference (Beare et al. 2006). Note that the LES results of the lowest three grid points (lowest 10 m in this case) are not reliable. As such the LES wind profile between 10 and 80 m (see Fig. 5b) can be described by

$$\overline{v}(z) = C\overline{v}_{MAX}\left(\frac{z}{h}\right)^p \left(1 - \frac{z}{h}\right)^q, \tag{8}$$

where C is a constant, $\overline{v}_{MAX}$ is the wind speed maximum in the layer, and p and q are fitting constants. Knowing that the derivative of $\overline{v}$ with respect to height is zero at $\overline{v}_{MAX}$, and by

using $p = 0.3$ and $q = 1$ together with the wind maximum of 3.1 m s^{-1} at 80 m, we arrive at $C = 2$. Integration of Eq. 3 with (7) then gives us this function for the height dependence of $\overline{u'w'}$:

$$\overline{u'w'} = fC\overline{v}_{MAX}h\left(\frac{z}{h}\right)^{p+1}\left(\frac{1}{(p+1)} - \frac{z}{h}\frac{1}{(p+2)}\right) + \overline{u'w'}_o. \tag{9}$$

This curve, using the above parameters, is shown in Fig. 7b, and follows the average LES results closely (above 10 m); it is clearly seen that the curve has a positive curvature close to the ground consistent with the strong variation of cross-isobaric wind component with height near the surface (as seen in Fig. 5).

The above analysis indicates that the simulated surface angle is determined by the details of the turbulence closure near the surface, which in turn influences the height of the stable boundary layer. Thus, it is important not only to examine the normalised total momentum flux, but also its components. In addition, the height to the first model level and the vertical resolution near the surface play a crucial role, since the curvature in the momentum profile cannot be resolved properly on a coarse grid. Indeed recent results over the ocean indicate that lowering the model level improves the wind turning angle (Brown et al. 2008).

4.3 Selected Model Results

From the above analysis, it becomes clear that an incorrect or inconsistent representation of the momentum profile close to the surface has a strong impact on the surface angle. Therefore, in Fig. 9a we redraw the surface angle as a function of h (similar as in Fig. 6), but excluding the models that have the indicated problems near the surface. Note that the omitted models do not derive from one type of turbulence parameterisation. After selection the scatter is reduced considerably and now a monotonic function appears between the two quantities. This result is consistent with the theory in Sect. 2. However, as can be seen in Fig. 9, there are only a few models consistent with the LES results for the surface angle and the boundary-layer depth. The models that deviate from the LES results (except one) have a boundary-layer scheme that produces excessive turbulent mixing.

In Fig. 9b the surface angle is presented as function of the boundary-layer depth normalised with values for the Obukhov length calculated for each model. This provides a rather similar organisation as Fig. 9a and also illustrates the variation in stability simulated by the models. In addition, Fig. 10 gives a redrawn Fig. 2 for the selected models only. Again the spread among the models is reduced, and the remaining differences are related to the differences in the turbulence schemes.

To further examine this, we compare the terms of Eq. 6 normalized with surface stress (Fig. 11); again the calculation is only performed for models that are included in Figs. 9 and 10. Most of the models then show good agreement between the two quantities presented, as the averaged LES, but some points are well above or below the 1:1 line. For some of the outliers, the wind vector does not return to the geostrophic wind vector, i.e. $v \neq 0$, above the boundary layer (see Figs. 1c and 5a).

In Fig. 12 the surface value of the momentum flux is plotted against the integral evaluated over the boundary-layer depth for the selected models. Overall the agreement is good between the two terms along the axis of Fig. 12, certainly in comparison with Fig. 11, which shows an alternative way of plotting between related variables (see text about Eqs. 5 and 6). Apparently, normalizing with the surface stress introduces additional scatter. However, in

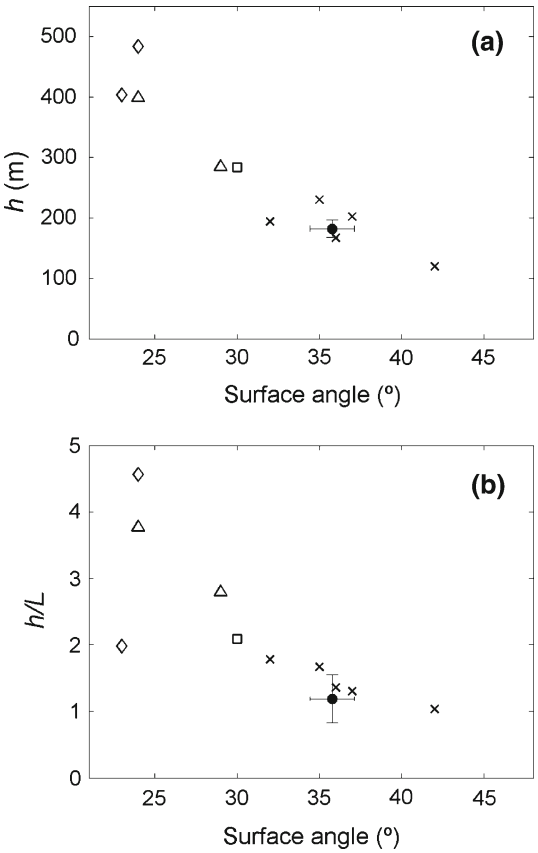

Fig. 9 **a** Similar as Fig. 6 for the models after selection. **b** Similar as Fig. 9a but boundary-layer depth normalised by the Obukhov length. See text for further discussion

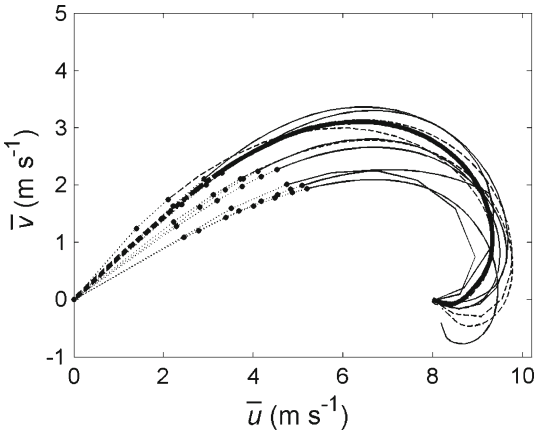

Fig. 10 Similar as in Fig. 2 for the models after selection

Fig. 12 there is also a tendency for the operational models to have a slightly larger magnitude of the integrated value than motivated by the surface value of the turbulent stress. This might be attributed to the accuracy of the representation of the integral on a coarser model grid.

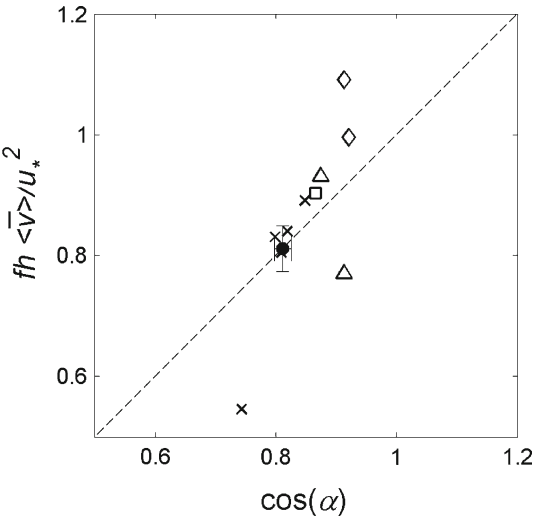

Fig. 11 The relation between the boundary-layer mean ageostrophic wind and the surface angle, according to Eq. 6 after selection. Symbols as in Fig. 4. See text for further discussion

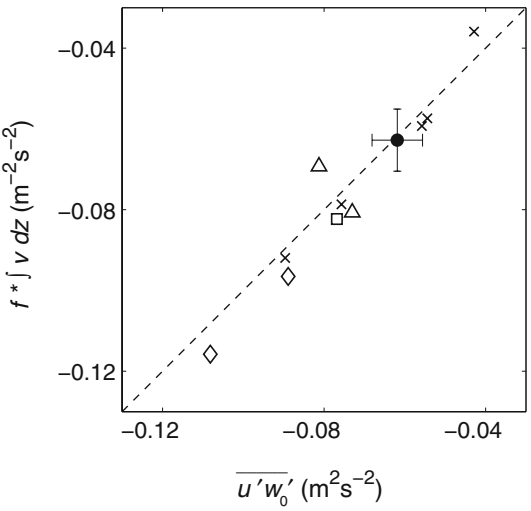

Fig. 12 The integrated cross-isobaric wind component plotted against the turbulent stress (at the two lowest model layers connected with a line) in the direction of the geostrophic wind after selection. Here the integral is evaluated over the boundary-layer height (See Eq. 5 left hand side). Symbols as in Fig. 4

5 Conclusions

In this study, a further analysis of model results from the first model intercomparison of the GEWEX Atmospheric Boundary Layer Study (GABLS) has been performed with the focus on the turning of wind with height and the related cross-isobaric (ageostrophic) flow. The experiment basically numerically solves the boundary-layer equations and the variations between the different single-column model results arise only from the different turbulence parameterisations (Cuxart et al. 2006). The single-column model results are compared with averaged LES results reported in Beare et al. (2006). The participating models range from first-order local schemes used in operational models to research models with higher-order closures (Cuxart et al. 2006).

The cross-isobaric flow within the boundary layer is produced by friction at the surface in the direction of the geostrophic wind. The layer that is affected by the surface is of variable

depth, with the operational weather forecast models having the deepest layers (Cuxart et al. 2006), i.e. their turbulence closure enhances the mixing. However, according to theory, the angle between the surface and the geostrophic wind directions is determined by the vertical divergence of the momentum flux in the direction of the geostrophic wind close to the surface. The present analysis reveals that the resulting surface angle is very sensitive to details of the shape of this component of the momentum flux profile near the surface, and it is shown that several models have difficulty in the correct representation of the near-surface momentum flux profiles. When these models are removed from the analysis, the remaining models show good agreement with theory and indicate a clear relation between the depth of the boundary layer and the surface angle.

The operational models with enhanced mixing and a deeper boundary layer also have a larger integrated cross-isobaric flux, where the difference between the lowest and the highest value is almost a factor of three. This obviously has consequences for the development of synoptic-scale disturbances (e.g. Beare 2007). But, as the theory depicts, a deeper layer also implies less turning of the wind at the surface. Thus, there are important implications for transport direction and wind speed within the boundary layer as represented in three-dimensional atmospheric models. The results presented here indicate that close attention has to be paid to the matching between the surface parameterisation and the boundary-layer scheme when designing and evaluating a boundary-layer model.

Our analysis further indicates that the simulated surface angle is determined by the details in the turbulence closure near the surface, which in turn influences the height of the stable boundary layer. Thus, it is important not to only examine the total momentum flux, but also its components. In addition, the height to the first model level and the vertical resolution near the surface play a crucial role since the curvature in the momentum profile cannot be resolved properly on a coarse grid.

The models analysed here give a wide range of surface angles for given identical forcing conditions. However, there are no observations available to determine how the boundary layer in the real atmosphere develops under these conditions (and surface heterogeneity may complicate matters even further). To further advance this subject, we recommend analysis of turbulent momentum flux observations in a geostrophic wind coordinate system.

Acknowledgements The authors recognize the contribution from all members in the GABLS community sharing ideas and results. Especially acknowledged are the groups participating with models and the scientists compiling the data-base for the first single-column intercomparison: J. Cuxart, R.J. Beare, E. Bazile, A. Beljaars, A. Cheng, L. Conangla, M. Ek, F. Freedman, R. Hamdi, A. Kerstein, H. Kitagawa, G. Lenderink, D. Lewellen, J. Mailhot, T. Mauritsen, V. Perov, G. Schayes, G.-J. Steeneveld, P. Taylor, W. Weng, S. Wunsch, and K.-M. Xu. We also thank R.J. Beare, S. Basu, J. Cuxart, T. Mauritsen, L. Mahrt, G.-J. Steeneveld, and M. Tjernström for valuable comments on drafts of this paper.

References

Andrén A (1990) Evolution of a turbulence closure scheme suitable for air-pollution applications. J Appl Meteorol 29:224–239. doi:10.1175/1520-0450(1990)029<0224:EOATCS>2.0.CO;2

Angevine WM, Tjernström M, Zagar M (2006) Modeling of the coastal boundary layer and pollutant transport in New England. J Appl Meteorol Climatol 45:137–154. doi:10.1175/JAM2333.1

Basu S, Porté-Agel F (2006) Large-eddy simulation of stably stratified atmospheric boundary layer turbulence: a scale-dependent dynamic modeling approach. J Atmos Sci 63:2074–2091. doi:10.1175/JAS3734.1

Beare RJ (2007) Boundary layer mechanisms in extratropical cyclones. Q J Roy Meteorol Soc 133:503–515. doi:10.1002/qj.30

Beare RJ, MacVean MK, Holtslag AAM, Cuxart J, Esau I, Golaz J-C, Jimenez MA, Khairoutdinov M, Kosovic B, Lewellen D, Lund TS, Lundquist JK, McCabe A, Moene AF, Noh Y, Raasch S, Sullivan

PP (2006) An intercomparison of large-eddy simulations of the stable boundary layer. Boundary-Layer Meteorol 118:247–272. doi:10.1007/s10546-004-2820-6

Blackadar AK (1957) Boundary layer wind maxima and their significance for the growth of nocturnal inversions. Bull Am Meteorol Soc 38:283–290

Bosveld F, Beyrich F (2004) Classifying observations of stable boundary layers for model validation. In: Sixteenth symposium on boundary layers and turbulence, Portland, Maine, US, 9–13 August

Brown AR, Beare RJ, Edwards JM, Lock AP, Keogh SJ, Milton SF, Walters DN (2008) Upgrades to the bounadry-layer scheme in the MetOffice numerical weather prediction model. Boundary-Layer Meteorol 128:117–132. doi:10.1007/s10546-008-9275-0

Caughey SJ, Wyngaard JC, Kaimal JC (1979) Turbulence in the evolving stable boundary layer. J Atmos Sci 36:1041–1052

Cuxart J, Holtslag AAM, Beare RJ, Bazile E, Beljaars A, Cheng A, Conangla L, Ek M, Freedman F, Hamdi R, Kerstein A, Kitagawa H, Lenderink G, Lewellen D, Mailhot J, Mauritsen T, Perov V, Schayes G, Steeneveld G-J, Svensson G, Taylor P, Weng W, Wunsch S, Xu K-M (2006) Single-column model intercomparison for a stably stratified atmospheric boundary layer. Boundary-Layer Meteorol 118:273–303. doi:10.1007/s10546-005-3780-1

Ekman VW (1905) On the influence of the earth's rotation on ocean-currents. Arkiv Matem, Astr Fysik Stockh 2(11)

Grisogono B, Oerlemans J (2001) Katabatic flow: Analytic solution for gradually varying eddy diffusivities. J Atmos Sci 58:3349–3354. doi:10.1175/1520-0469(2001)058<3349:KFASFG>2.0.CO;2

Holton JR (2004) An introduction to dynamic meteorology, 4th edn. Elsevier Academic Press, Amsterdam, 535 pp

Holtslag AAM (2003) GABLS initiates intercomparison for stable boundary layers. GEWEX News 13:7–8

Holtslag AAM (2006) GEWEX Atmospheric Boundary-Layer Study (GABLS) on stable boundary layers. Boundary-Layer Meteorol 118:243–246. doi:10.1007/s10546-005-9008-6

Holtslag AAM, Nieuwstadt FTM (1986) Scaling the atmospheric boundary layer. Boundary-Layer Meteorol 36:201–209. doi:10.1007/BF00117468

Kosovic B, Curry JA (2000) A large eddy simulation study of a quasi-steady, stably stratified atmospheric boundary layer. J Atmos Sci 57:1052–1068. doi:10.1175/1520-0469(2000)057<1052:ALESSO>2.0.CO;2

Lundquist JK (2003) Intermittent and elliptical inertial oscillations in the atmospheric boundary layer. J Atmos Sci 60:2661–2673. doi:10.1175/1520-0469(2003)060<2661:IAEIOI>2.0.CO;2

Nieuwstadt FTM (1984) The turbulent structure of the stable boundary layer. J Atmos Sci 41:2202–2216. doi:10.1175/1520-0469(1984)041<2202:TTSOTS>2.0.CO;2

Nieuwstadt FTM (1985) A model for the stationary, stable boundary layer. In: Turbulence and diffusion in stable environments. Hunt JCR (ed), Clarendon Press, Oxford, pp 149–179

Parmhed O, Kos I, Grisogono B (2005) An improved Ekman layer approximation for smooth eddy diffusivity profiles. Boundary-Layer Meteorol 115:399–407. doi:10.1007/s10546-004-5940-0

Stull R (1988) An introduction to boundary layer meteorology. Kluwer Academic Publishers, Dordrecht, 670 pp

Tan Z-M (2001) An approximate analytical solution for the baroclinic and variable eddy diffusivity semi-geostrophic Ekman boundary layer. Boundary-Layer Meteorol 98:361–385. doi:10.1023/A:1018708726112

van Ulden AP, Holtslag AAM (1985) Estimation of atmospheric boundary layer parameters for diffusion applications. J Appl Meteorol 24:1196–1207. doi:10.1175/1520-0450(1985)024<1196:EOABLP>2.0.CO;2

Walcek CJ (2002) Effects of wind shear on pollution dispersion. Atmos Environ 36:511–517. doi:10.1016/S1352-2310(01)00383-1